Journal of Applied Fluid Mechanics, Vol. 12, No. 2, pp. 515-526, 2019.
Available online at www.jafmonline.net, ISSN 1735-3572, EISSN 1735-3645.
DOI: 10.29252/jafm.12.02.29018

Combined Heat and Mass Transfer during Condensation of Vapours Mixture and Non-Condensable Gas in a Vertical Tube

A. Charef†, M. Feddaoui, A. Nait Alla and M. Najim

GEMS Laboratry, Ibn Zohr University, ENSA B.P. 1136, Agadir, Morocco

†*Corresponding Author Email: adil.charef@edu.uiz.ac.ma*

(Received March 17, 2018; accepted September 24, 2018)

ABSTRACT

The problem of laminar film condensation from binary vapours mixture with the presence of non-condensable gas (air) flowing in a vertical tube is numerically investigated. The set of the non-linear parabolic equations expressing the mass conservation, momentum, energy, and species diffusion in both phases with the boundary conditions are resolved by using a finite difference numerical scheme. A comparative study between the results obtained for three cases (water-ethanol-air, water-methanol-air, and ethanol-methanol-air) under the same conditions is made. The impact of varying the wall temperature, the inlet vapour mass fractions, and the inlet liquid mass flow rate on the conjugate the heat and mass transfer during the condensation of the studied mixtures are examined. It is found that the condensation of water-methanol-air corresponds to a higher latent heat flux Q_{L2} and accumulated condensation rate Mr2 when compared with water-ethanol-air and ethanol-methanol-air. Moreover, the nature of the fluid plays an important role in the heat and mass exchanges.

Keywords: Condensation; Liquid film thickness; Laminar flow; Phase change; Vertical tube.

NOMENCLATURE

C_p	specific heat
D	diffusion coefficient
d	diameter of the tube d=2R
h_{fg}	latent heat of condensation
h_T	heat transfer coefficient
J''_i	heat flux of species i at the interface
m_{0G}	inlet has mass flow rate
Mr	total accumulated condensation rate
Q_L	latent heat flux
Q_S	sensible heat flux
Q_{Li}	latent heat flux of species i
w_{0Li}	liquid mass flux of species i
w^*	dimensionless vapour mass fraction
$Y_{L,I}$	molar fraction for species in the liquid film
δ	liquid film thickness
ʎ	thermal conductivity
μ	dynamic viscosity
ρ	density
τ	shear stress
ϕ	relative humidity

Subscripts

0	condition at the inlet of the tube
a	referring to the air
am	dry air in the mixture
G	referring to the vapour-gas mixture
im	species I in the mixture
I	interface
L	referring to the liquid

1. INTRODUCTION

Liquid film condensation of multicomponent mixed vapours are extensively encountered in many industrial sectors. In the chemical processing or distillation, it is often an effective way to separate the binary composed of vapour alcohols with the presence of air. Controlling the concentration from the aqueous solutions at the exit of the condensers in the presence of a liquid film passes through the accurate knowledge of heat and mass transfer between the liquid and the gas mixture. The study of water vapour condensation arouses the interest of many authors and gives place to numerous studies thanks to the availability of this source and its relatively weak cost in comparison to other fluids.

The condensation of water vapour has received special attention in many experimental and theoretical studies. Siow *et al.* (2004) performed numerically a laminar condensation of steam-air in a vertical channel. Their analysis demonstrates that a larger air concentration reduces considerably the thickness of the condensate film, Nusselt number and pressure gradient. Belhadj *et al.* (2007) investigated numerically the condensation mechanism of steam-air along a vertical channel. They showed that the phenomenon of the phase change is extremely sensitive to the liquid film temperature. For various values of the system parameters at the tube inlet, Dharma *et al.* (2008) examined numerically the pressure drop, the local and average values of Nusselt number, the film Reynolds number and the interface temperature. Also, Hassaninejadfarahani *et al.* (2014) reported detailed investigations on the liquid film condensation of steam-air in a vertical tube. Their results include the effects of the inlet relative humidity, the inlet air mass fraction, the inlet Reynolds number and the tube radius on the conjugate heat and mass transfer. Kubin *et al.* (2016) presented an experimental study during steam condensation in a small diameter of vertical tube. They used the methods of thermal resistance and Wilson plot to calculate the condensation heat transfer coefficient.

As far as the condensation of multicomponent vapours is concerned, Taitel and Tamir (1974) performed an analytical study of the film condensation for three component systems of methanol-water-air on a vertical plate. They noticed a decrease in the interface temperature and the condensation rate with an increase in the non-condensable gas or the accumulation of the more volatile components at the interface vapour-liquid. Krishna and Panchal (1977) analyzed the heat and mass transfer during the condensation of methanol and water vapours with the presence of air. They showed that diffusional interactions considerably affect the process of condensation. Later, Krishna (1979) studied the effect of the composition and the nature of non-condensable gas on the condensation of methanol-water vapour mixture. Utaka *et al.* (2004) studied the effect of mixing vapour ethanol and steam on the process of condensation. Their results show that the condensation heat transfer is improved compared with the pure steam. Li *et al.* (2008) found experimentally from the condensation of water-ethanol mixture on vertical tube that with lower concentration of ethanol, the heat transfer coefficient becomes higher. Wang *et al.* (2009) examined water-ethanol condensation within a large range of ethanol concentration inside vertical surface. They showed that by increasing the pressure and vapour velocity, the heat transfer coefficient is improved. Ma *et al.* (2012) conducted an experimental study in the case of condensation from steam-ethanol mixture. They analyzed the impact of surface free energy difference and subcooling on the coefficient of heat transfer. Jiang *et al.* (2015) presented the results of an experimental investigation during the condensation of ethanol-water. They measured the ethanol concentration variation and the distribution of steam quality in trapezoidal microchannel.

To the author's knowledge, no computational study has been conducted concerning the condensation of the binary liquid film taking into account the mass diffusion in both phases. The present study is made to uncover the condensation mechanism especially with the presence of non-condensable gas, which finds tremendous application in the separation processes. In fact, by adding mass diffusion in the liquid phase, we can examine the binary liquid film condensation from multicomponent mixed vapours. This motivates us in the current study to analyze the simultaneous heat and mass transfer during the condensation of the three cases: water-ethanol-air, water-methanol-air, and ethanol-methanol-air, respectively.

2. MATHEMATICAL ANALYSIS

The geometry of the problem under consideration is shown schematically in Fig. 1. A mixture of water-ethanol, water-methanol or ethanol-methanol vapours and non-condensable gas enters a vertical tube of radius R and length L with uniform parameters (temperature T_0, mass flow rate m_{0G}, and mass fraction w_{0i}). The external tube wall is maintained at T_W. A binary liquid film condensation flowing downward with an inlet liquid temperature T_{0L}, inlet liquid mass flow rate m_{0L}, and inlet liquid mass fraction of w_{0Li}.

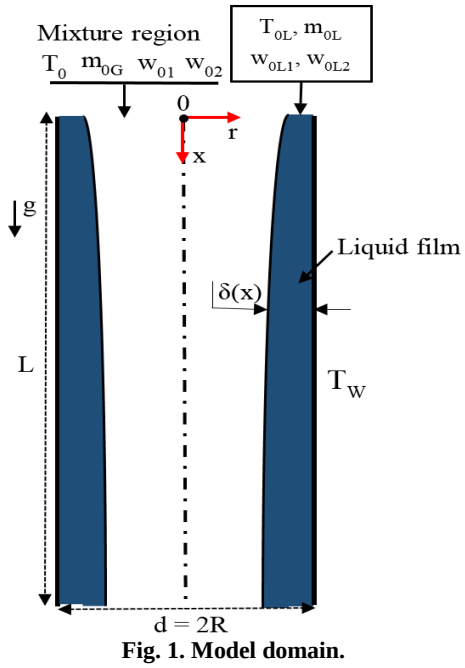

Fig. 1. Model domain.

In the mathematical model, it is assumed that the flow in both phases is laminar, axisymmetric, incompressible and steady. The liquid-mixture interface is in thermodynamic equilibrium. The axial diffusion of heat, mass and momentum are negligible (Feddaoui *et al.* (2001)); that the heat transfer by the radiation, Soret and Dufour effects are negligible (Armou *et al.* (2017)). Finally, the

gas and the liquid phases have the same pressure.

2.1 Governing Equations

The governing equations for the liquid film, the gas phase, boundary and interfacial conditions are given below:

Basic equations for the liquid film

$$\frac{\partial}{\partial x}(\rho_L u_L)+\frac{1}{r}\frac{\partial}{\partial r}(r\rho_L v_L)=0 \tag{1}$$

$$\frac{\partial}{\partial x}(\rho_L u_L u_L)+\frac{1}{r}\frac{\partial}{\partial r}(r\rho_L v_L u_L)=-\frac{dP_d}{dx}+\frac{1}{r}\frac{\partial}{\partial r}(r\mu_L\frac{\partial u_L}{\partial r})+(\rho_L-\rho_0)g \tag{2}$$

$$\frac{\partial}{\partial x}(\rho_L u_L C_{pL} T_L)+\frac{1}{r}\frac{\partial}{\partial r}(r\rho_L v_L C_{pL} T_L)=\frac{1}{r}\frac{\partial}{\partial r}(r\lambda_L\frac{\partial T_L}{\partial r})+\frac{\partial}{\partial r}\frac{1}{r}\left[r\rho_L D_L\left(C_{pL,1}-C_{pL,2}\right)T_L\frac{\partial w_{L1}}{\partial r}\right] \tag{3}$$

$$\frac{\partial}{\partial x}(\rho_L u_L w_{Li})+\frac{1}{r}\frac{\partial}{\partial r}(r\rho_L v_L w_{Li})=\frac{1}{r}\frac{\partial}{\partial r}(r\rho_L D_L\frac{\partial w_{Li}}{\partial r})\qquad i=1,2 \tag{4}$$

Basic equations for the gas phase

Similarly, in the gas region, the governing equations are those of continuity, momentum, energy, and species diffusion, respectively.

$$\frac{\partial}{\partial x}(\rho_G u_G)+\frac{1}{r}\frac{\partial}{\partial r}(r\rho_G v_G)=0 \tag{5}$$

$$\frac{\partial}{\partial x}(\rho_G u_G u_G)+\frac{1}{r}\frac{\partial}{\partial r}(r\rho_G v_G u_G)=-\frac{dP_d}{dx}+\frac{1}{r}\frac{\partial}{\partial r}(r\mu_G\frac{\partial u_G}{\partial r})+(\rho_G-\rho_0)g \tag{6}$$

$$\frac{\partial}{\partial x}(\rho_G u_G C_{pG} T_G)+\frac{1}{r}\frac{\partial}{\partial r}(r\rho_G v_G C_{pG} T_G)=\frac{1}{r}\frac{\partial}{\partial r}(r\lambda_G\frac{\partial T_G}{\partial r})+\sum_{i=1}^{2}\frac{1}{r}\frac{\partial}{\partial r}\left[r\rho_G\left(D_{G,im}C_{pG,i}-D_{G,am}C_{pG,a}\right)T_G\frac{\partial w_{Gi}}{\partial r}\right] \tag{7}$$

$$\frac{\partial}{\partial x}(\rho_G u_G w_{Gi})+\frac{1}{r}\frac{\partial}{\partial r}(r\rho_G v_G w_{Gi})=\frac{1}{r}\frac{\partial}{\partial r}(r\rho_G D_{G,im}\frac{\partial w_{Gi}}{\partial r})\qquad i=1,2,a \tag{8}$$

Where P_d is the dynamic pressure. The pressure gradient in Eq. 6 can be written as: $\frac{dP}{dx}=\frac{dP_d}{dx}+\rho_0 g$.

Thus, the term: $-\frac{dP}{dx}+\rho g=-\frac{dP_d}{dx}+(\rho_G-\rho_0)g$.

The term $(\rho_G-\rho_0)$ is the buoyancy forces because of the variations of concentration and temperature.

2.2 Boundary and Interfacial Conditions

In the present model, the boundary conditions subject for Eqs (1) - (8) are given as follows:

At the inlet of the tube (x = 0)

$$m_L=m_{0L};T_L=T_{0L};w_{Li}=w_{0Li} \tag{9}$$

$$m_G=m_{0G};T_G=T_0;P_d=0;w_{Gi}=w_{0i} \tag{10}$$

To compare the results of the three cases, it is useful to have the same gas flow at the tube inlet, for this reason, m_{0G} is given. The inlet velocity $u_0=\frac{m_{0G}}{\pi\rho_0(R-\delta_0)^2}$ and the inlet Reynolds number Re_0 are calculated to be certain that our model is in laminar region.

At the center line (r = 0)

$$v_G=0;\frac{\partial u_G}{\partial r}=0;\frac{\partial T_G}{\partial r}=0;\frac{\partial w_{Gi}}{\partial r}=0\quad i=1,2,a \tag{11}$$

At the tube wall (r = R)

$$u_L=v_L=0;T_L=T_W;\frac{\partial w_{Li}}{\partial r}=0\quad i=1,2 \tag{12}$$

At the liquid-mixture interface (r = R-δ_x)

Continuities of temperature, velocity and shear stress

$$T_I(x)=T_{G,I}=T_{L,I};u_I(x)=u_{G,I}=u_{L,I} \tag{13}$$

$$\tau_I=\left[\mu\frac{\partial u}{\partial r}\right]_{L,I}=\left[\mu\frac{\partial u}{\partial r}\right]_{G,I} \tag{14}$$

- Heat balance at the interface implying (Charef *et al.* (2017)).

$$\left[\lambda\frac{\partial T}{\partial r}\right]_{L,I}=\left[\lambda\frac{\partial T}{\partial r}\right]_{G,I}-J^{"}h_{fg} \tag{15}$$

Where hfg is the latent heat of vaporization, and $J^{"}$ is the mass flux at the interface $\left(J^{"}=\rho_G v_I\right)$.

Along the interface, the heat transfer can be made by the latent and sensible modes owing to the partial condensation of vapours. Thus, the total convective heat transfer is defined by:

$$Q_T=Q_S+Q_L=\left[\lambda\frac{\partial T}{\partial r}\right]_{G,I}-J^{"}h_{fg} \tag{16}$$

Mass conservation at the interface:

The continuity of the condensed flows of each constituent at the interface is given as follows:

$$J_i^{"} = J^{"} w_{Li} - \rho_L D_{L,12} \frac{\partial w_{Li}}{\partial r} = J^{"} w_{Gi} - \rho_G D_{G,im} \frac{\partial w_{Gi}}{\partial r} \qquad i = 1,2 \tag{17}$$

The radial velocity of steam-air mixture at the interface is calculated as follows:

$$v_I = -\frac{\sum_{i=1}^{2} D_{G,im} \frac{\partial w_{Gi}}{\partial r}}{\left(1 - \sum_{i=1}^{2} w_{Gi}\right)} \tag{18}$$

Owing to Dalton's law, and by considering that the steam-air mixture is ideal gas, the interfacial concentrations w_{Gi} in the gas phase can be calculated by using the same equations given in Nasr et al. (2011a; 2017b; 2017c) as follows:

$$w_{G1} = \frac{M_1 P_{v,1}^*}{M_1 P_{v,1}^* + M_2 P_{v,2}^* + \left[P - P_{v,1}^* - P_{v,2}^*\right] M_a} \tag{19}$$

$$w_{G2} = \frac{M_2 P_{v,2}^*}{M_2 P_{v,2}^* + M_1 P_{v,1}^* + \left[P - P_{v,1}^* - P_{v,2}^*\right] M_a} \tag{20}$$

Where M_i and M_a are the molar masses of vapour i and air, respectively. $P_{v,I}^* = Y_{L,i} P_{v,i}$ is the partial pressure of vapour at the interface. $Y_{L,i}$ is the molar fraction for species i in the liquid film. $P_{v,i}$ is the pressure of saturated vapour of species i.

The governing Eqs. (1) - (8) with interfacial conditions (9) - (16) are used to determine the field of variables $u_L, v_L, T_L, w_{Li}, u_G, v_G, T_G, w_{Gi}$. To complete the mathematical model, two equations are used. At each axial location, the overall mass balance in the gas region and the liquid film (Najim *et al.* (2017)) should be satisfied:

$$\frac{m_{0L}}{2\pi} = \int_{R-\delta_x}^{R} \left(r \rho u dr\right)_L - \int_0^x \rho_G v_I \left(R - \delta_x\right) dx \tag{21}$$

$$\frac{\left(R - \delta_0\right)^2}{2} \rho_0 u_0 = \int_0^{R-\delta_x} \left(r \rho u dr\right)_G + \int_0^x \rho_G v_I \left(R - \delta_x\right) dx \tag{22}$$

Nusselt number for latent heat is defined as:

$$Nu_L = \frac{J^{"} h_{fg} \left(2R\right)}{\lambda_G \left(T_b - T_I\right)} \tag{23}$$

The bulk temperature T_b is given by:

$$T_b = \frac{\int_0^{R-\delta_x} \left(r \rho C_P u T\right)_G dr}{\int_0^{R-\delta_x} \left(r \rho C_P u\right)_G dr} \tag{24}$$

For a better understanding of the heat and mass transfer, the accumulated condensation rate of species i *Mri* and total accumulated condensation rate *Mr* are written as:

$$Mri = \frac{2\pi \int_0^x J_i^{"} \left(R - \delta_x\right) dx}{m_{0G}}; Mr = \frac{2\pi \int_0^x J^{"} \left(R - \delta_x\right) dx}{m_{0G}} \tag{25}$$

To fix gas-liquid interface, the cylindrical coordinate is transformed into η coordinate system as:

$$\eta = \frac{\left(R - \delta_x\right) - r}{\left(R - \delta_x\right)} \quad 0 < r < \left(R - \delta_x\right) \tag{26}$$

$$\eta = \frac{\left(R - \delta_x\right) - r}{\delta_x} \quad \left(R - \delta_x\right) < r < R \tag{27}$$

The pure component data is approached by polynomials in terms of mass fraction and temperature. For more information, the thermo-physical properties are available in Appendix A, [(Poling *et al.* (2001)), (Perry *et al.* (1997))].

3. NUMERICAL METHOD

In the present problem, the non-linear parabolic Eqs. (1) - (8) with the boundary conditions are solved numerically by a fully implicit scheme. Each finite-difference equation's system forms a tridiagonal matrix, which can be resolved by the Thomas-algorithm (Patankar (1980)). The axial convection terms are approached using a backward difference. The transversal diffusion and convection terms are approached using a central difference.

In the centreline, the Hospital's rule is utilized to get a correct representation of the diffusional terms notably for the heat flow and shear stress. At every location, the axial velocity profile and pressure gradient corrections are made by Raithby and Schneider (1979), which is described by Anderson *et al.* (1984). Moreover, to enhance numerical solutions accuracy, a non-uniform grid is employed for axial and radial directions.

In order to avoid convergence problems resulting from the use of thin grids, it is helpful to find the optimum solutions between the precision and computing time. Figure 2(a-b) shows the grid independency test for local Nusselt number for five combinations of grid sizes. It is found that the grid nodes number in two cases (case 1 and case 3) has no effect on the computations accuracy. In the light of those results, the grid $N_I \times (N_J + N_K) = 131 \times (81+31)$ is chosen to gain the computation time and precision. Note that N_I: total grid points in the flow direction; N_J: grid points in the transversal direction at the gas phase; N_K: grid points in the transversal direction at the liquid phase.

3.1. Marching Procedure

After the initialization of both liquid and gas inlet values, the numerical computation is advanced forward and step by step as follows:

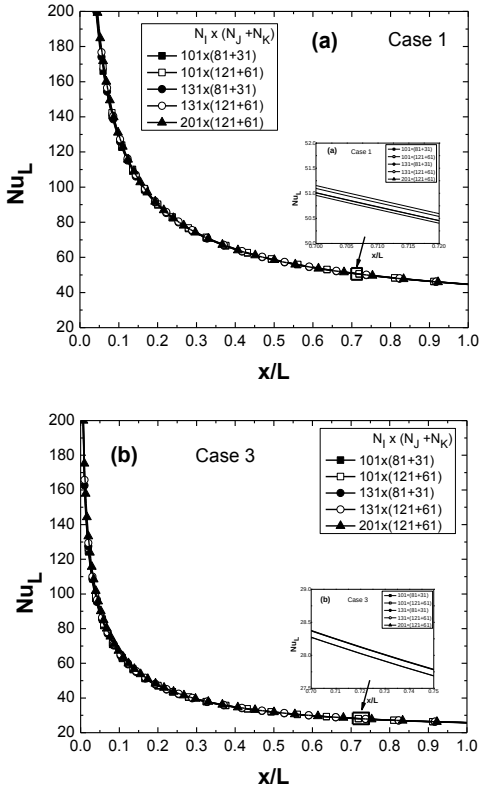

Fig. 2. Comparison of local Nusselt number for various grid arrangements (T_W = 5 °C, T_0 = 100 °C, w_{01} = w_{02} = 0.25, L = 0.5 m, P_0 = 1 atm) for case 1 (a), case 3 (b).

For I = 1, the liquid film longitudinal velocity is given by resolving the momentum balance equation neglecting the convection and inertia terms. Initially, the film thickness is calculated by :

$$\delta_0 = \left(\frac{3\mu_L m_{0L}}{\rho_L^2 g} \right)^{\frac{1}{3}} \tag{28}$$

For I = 2 to N_I:

1) In the first iteration, an arbitrary value of pressure gradient $\frac{dP_d}{dx}$ and liquid film thickness δ_x^{itt} are assumed.

2) Solve the finite difference forms of Eqs. (2) - (4) and (6) - (8) simultaneously for u_L, u_G, T_L,T_G, w_{Li}, w_{Gi}.

3) The continuities of velocity, temperature, shear stress and mass fraction of each species i at the interface are obtained from equations (13) to (20).

4) Numerically integrate the continuities Eqs. (1) and (5) to find v_L and v_G.

5) Calculate the error of the liquid film mass balance E_L^{itt} using Eq. (21).

6) For the thickness of the liquid film, a best approximation is calculated by the secant method (Ralson (2001)). Thus:

$$\delta_x^{itt+1} = \delta_x^{itt} - \frac{\delta_x^{itt} + \delta_x^{itt-1}}{E_L^{itt} - E_L^{itt-1}} E_L^{itt} \tag{29}$$

The convergence criteria used is $E_L^{itt} = 10^{-4}$. Usually six to seven iterations suffice to get converged solution.

7) Calculate the error in the gas flow balance E_G^{itt} using Eq. (22).

8) For the pressure gradient, a best approximation is obtained by the secant method. Thus:

$$\frac{dP_d}{dx}^{itt+1} = \frac{dP_d}{dx}^{itt} - \frac{\frac{dP_d}{dx}^{itt} - \frac{dP_d}{dx}^{itt-1}}{E_G^{itt} - E_G^{itt-1}} E_G^{itt} \tag{30}$$

9) Check the satisfaction of the convergence of velocity, temperature and species concentrations. If the relative error between two consecutive iterations is small enough, i.e.:

$$E_{rr} = \frac{\max\left| \Upsilon_{i,j}^n - \Upsilon_{i,j}^{n-1} \right|}{\max\left| \Upsilon_{i,j}^n \right|} < 10^{-4} \tag{31}$$

The solution for the actual axial position is complete. If not, repeat procedures (1) to (9). Where Υ represents the variables u_L, u_G, T_L,T_G, w_{Gi} and w_{Li}.

3.2. Comparison with Previous Studies

In order to check the accuracy and validity of the numerical method, the predictions of the present model were first compared with the study of Hassaninejadfarahani *et al.* (2014) for the case of laminar film condensation in the presence of air along a vertical tube. A better agreement is found between the current computational study and the results provided in the two studies as shown in Fig. 3(a, b), which illustrates the evolution of the water vapour mass fraction at the tube exit and the axial variation of the mixture temperature, respectively.

The second comparison with the study of Dharma *et al.* (2008) is based on the average Nusselt number of sensible heat at different values of Reynolds numbers for: ϕ_0 = 100 %, T_0 = 60 °C, T_W = 5 °C, L = 0.6m is presented. Figure 3c shows an excellent agreement between our prediction and those of Dharma *et al.* (2008). Moreover, the numerical simulation has similar trends with experimental data of Lebedev *et al.* (1969). Through these program tests and successful comparisons, we conclude that the model and the present numerical algorithm are suitable for the practical purpose. In fact, the present model can be applicable to other fluids than water such as alcohols or refrigerants, in which we can change only the thermo-physical properties of the studied fluids.

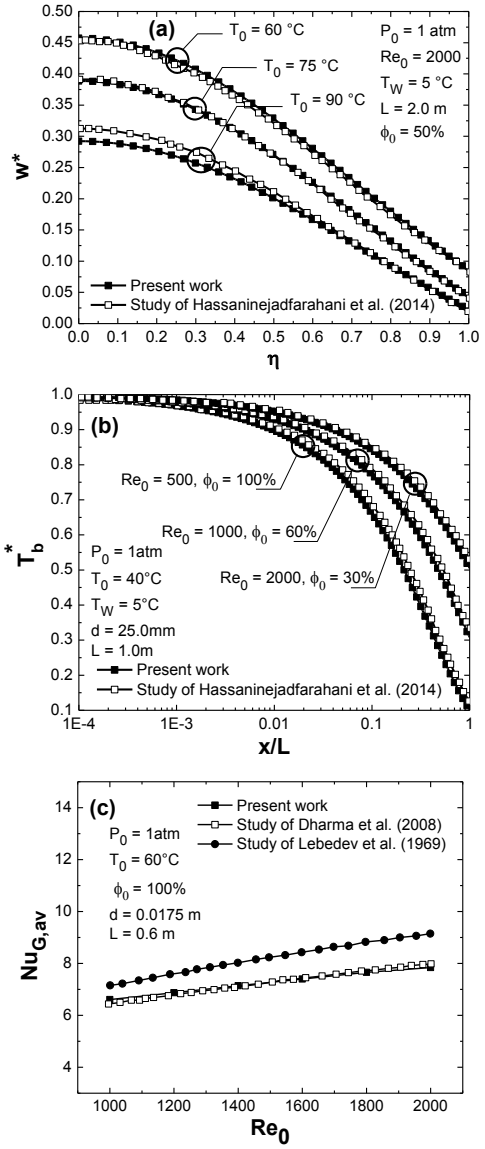

Fig. 3. Comparison with Hassaninejadfarahani *et al.* (2014) for the vapour mass fraction at the exit of the tube (a), for the dimensionless bulk temperature (b), comparison with Dharma *et al.* (2008) and Lebedev *et al.* (1969) for average Nusselt number of sensible heat (c).

4. Results and Discussion

Results were obtained for three cases: water-ethanol-air, water-methanol-air, and ethanol-methanol-air, respectively, which entering the tube with inlet vapour mass fractions of 0.4 - 0.5; inlet liquid mass flow of 1.0 $g.m^{-1}s^{-1}$ - 8.0 $g.m^{-1}s^{-1}$. In all cases, the inlet pressure is 1atm, inlet gas temperature of 100°C, inlet mass flow rate of 0.3 g/s, wall temperature is 5°C, inlet liquid temperature is 20°C, and the tube radius is 10.0 mm.

4.1. Physical Properties Variation

For comparing the condensation of multicomponent mixed vapours, it is seems more effective to investigate the variation of some physical properties, which have a great impact on the condensation process. Figure 4(a) presents a comparison of saturated pressure Psat for two alcohols: ethanol and methanol with water. It is noticed that the saturated pressure of methanol and ethanol are more important than water. Consequently, alcohols are more volatile than water. Another ascertainment is that when the temperature increases, Psat increases too especially for methanol. Figure 4(b) shows the variation of the latent heat of the condensation hfg as function of temperature. The first finding is that hfg decreases with the increase of temperature for all cases. Furthermore, water presents higher hfg than methanol and ethanol, respectively. This behavior means that the amount of heat per unit requires to elevate or decrease the temperature by one degree for water is more important than others.

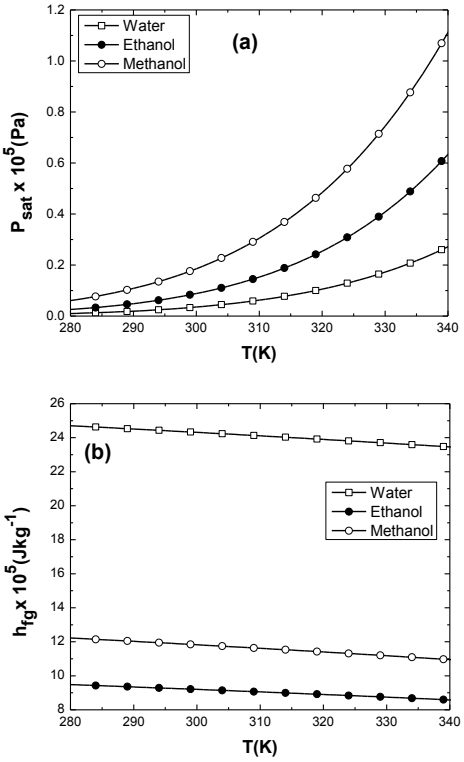

Fig. 4. Evolution of thermo-physical properties of the three fluids with temperature.

4.2. Distribution of the Vapour Mass Fractions W_{0i}

The distributions of axial vapour mass fraction profiles w_{0i} of the three cases along the tube are illustrated in Fig. 5. Figure 5 represents the evolution of the vapour mass fractions w_{01} and w_{02} in the gas phase for the three cases (water-ethanol-air, water-methanol-air and ethanol-methanol-air) at different sections of the tube. According to the results of these cases, the mass fractions of both species decrease from the centerline to the interface ($\eta = 0$). Also, it is observed that for all considered position, w_{01} and w_{02} of the three cases gradually decrease as the gas mixture progresses to the tube

exit. The results reveal that only the condensed vapour of the cases 1, 2 and 3 permeates the interface without air. Besides, by comparing the case 1 and 2, it is noted that w_{02} of case 2 diminishes more especially near the exit of the tube (X = 0.9). This diminution results from a higher condensation rate, which leads to the lowest residual vapour along the tube. It is also remarked that the mass fraction at the exit of the tube is less important during the condensation of w_{01} according to the mass diffusion coefficient of water vapour in the non-condensable gas, which is greater than that of methanol and ethanol, respectively. As opposed to the two cases, the condensation process of case 3 is lower for all axial positions owing to a weak total heat transfer to the condensate film.

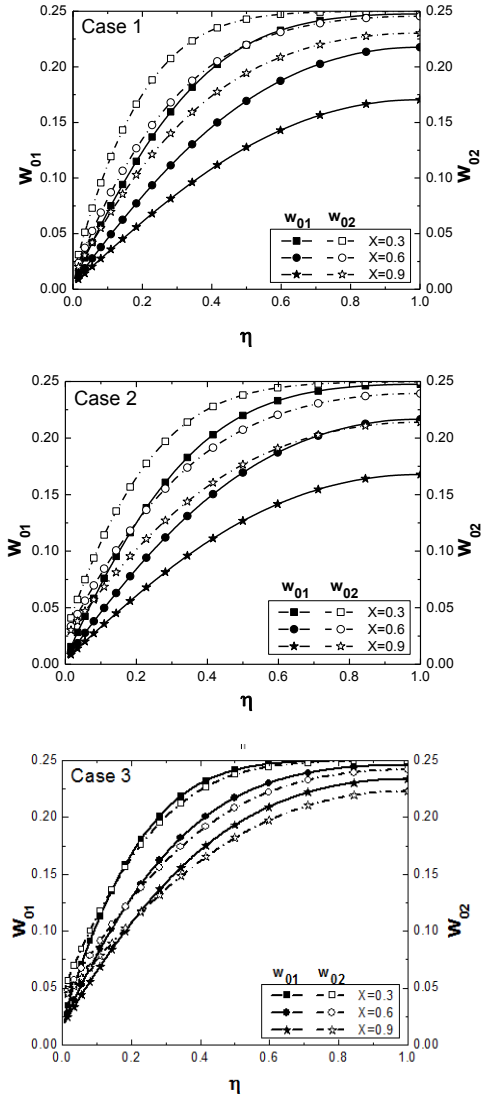

Fig. 5. Distribution of axial vapour mass fractions w_{01} and w_{02} for the three cases at different sections of the tube.

4.3. Distribution of the Vapour Mass Fractions W_{0i}

To evaluate the condensation rate of the alcohol vapour in the mixture, we have plotted the evolution of the accumulated condensation rate of alcohol Mr2 as a function of its vapour mass fraction w_{02}. Figure 6 presents the effect of varying the inlet vapour mass fractions w_{02} and wall temperature T_W on the accumulated condensation rate at different positions. It is interesting to observe that the curves of all cases show similar trends. For a fixed T_W, it is noted that an increase of the inlet vapour mass fraction w_{02} causes an increase of Mr2 along the tube. This result can be justified by the fact that the air mass fraction falls as the condensation rate rises, which improves the process of condensation according to the increase of the vapour concentration gradient at the liquid-gas interface, as seen in Fig. 5. In addition, the second case presents a higher Mr2 compared with case 1 and case 3, respectively. This is due to the much greater mass flux at the interface, which suggests that the mass transfer of case 2 resulting from latent heat exchanges is much more effective than other cases (seen later in Fig. 7). Furthermore, we observe that by decreasing T_W, accumulated condensation rate of water-ethanol-air is greater than that of water-methanol-air and ethanol-methanol-air, respectively (Mr2 of case 2 is approximately 8.5 % higher at the outlet of the tube by decreasing T_W from 20 to 5°C). This behavior is due to the higher amount of the condensed vapour with heat transfer increasing especially at the tube exit. This accounts for why condensation is enhanced for a higher temperature differences (T_0 - T_W).

4.4. Effect of the Inlet Vapour Mass Fractions W_{0i}

For a more detailed analysis of the heat and mass transfer characteristics during the condensation of water-ethanol-air, water-methanol-air or ethanol-methanol-air in a vertical tube. Our attention is focused on the effect of inlet vapour mass fraction w_{0i} on the latent heat flux Q_{L2} and the accumulated condensation rate Mr2 of species 2. Figure 7 presents the axial variations of the latent heat flux along the tube for all cases. According to the figure, the curves indicate that latent heat fluxes Q_{L2} of the three cases are very important at the inlet of the tube, then gradually decrease as the vapour-gas mixture passes through the tube and becomes almost constant beside the exit. This decrease in Q_{L2} is a result of the loss of vapour due to the end of condensation. It is also of interest to note that, for a fixed w_{01}, increasing w_{02} raises substantially the latent heat flux of case 2 than the others. This can be a result of reducing the air mass fraction at the interface, which enhances the heat and mass exchanges along the tube. Moreover, the diffusion coefficient of methanol in the non-condensable gas is bigger than that of ethanol, which promotes the condensation of case 2. However, by keeping the same air mass fraction (varying only w_{01} and fixing w_{02}), it can be seen that the air has a great influence on the condensation of a weak available amount of vapour w_{02}, which reduces the mass transfer mainly for case 3. This ascertainment is confirmed by Fig. 8, which represents axial variation of the accumulated condensation rate Mr2 for all cases. It is remarked that for a fixed w_{01}, Mr2 is reduced with decreasing w_{02}. Indeed, a weak vapour mass

fraction (higher air concentration) leads to a decrease of the accumulated condensation rate of all cases at the interface as a result of the presence of air, which plays the role of a resistance to mass transfer to the liquid film. Moreover, it is interesting to note that water-methanol-air present a larger accumulated condensation rate Mr2 than water-ethanol-air and ethanol-methanol-air (the growing is about 9.4 and 15.5 % at the outlet of the tube when w_{02} = 0.35). Note that the heat transfer during the condensation of all the cases depends on two interdependent phenomena: the sensible heat transfer caused by the difference of the temperature between the mixture region and the wall, and the latent heat transfer because of the alcohol vapour mass fraction w_{02} difference. For this reason, it is shown that a lower value of w_{02} of the three cases reduces the alcohol vapours content of the mixture especially at the inlet. Accordingly, the latent heat transfer to the condensate film decreases, which leads to a weak condensation along the tube. Furthermore, an increase in w_{01} slightly improve the accumulated condensation rate Mr2.

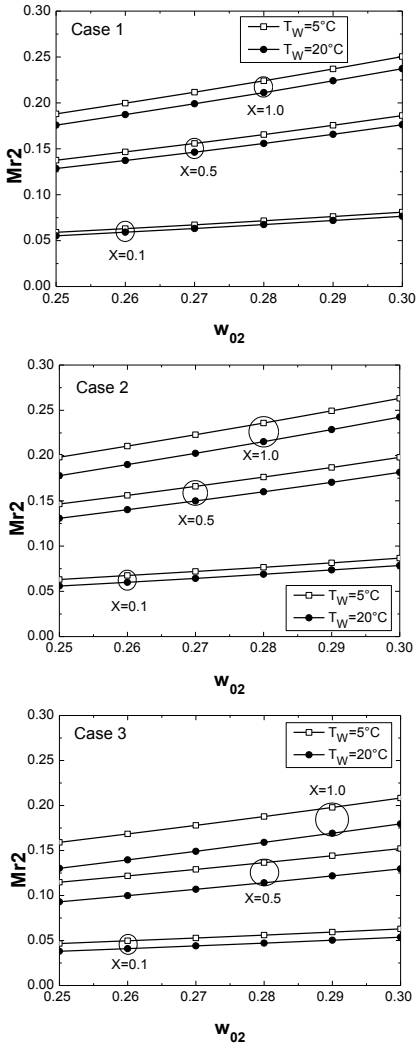

Fig. 6. Effect of inlet vapour mass fraction w_{02} and wall temperature T_W on the accumulated condensation rate of alcohols Mr2 at different sections of the tube for the three cases.

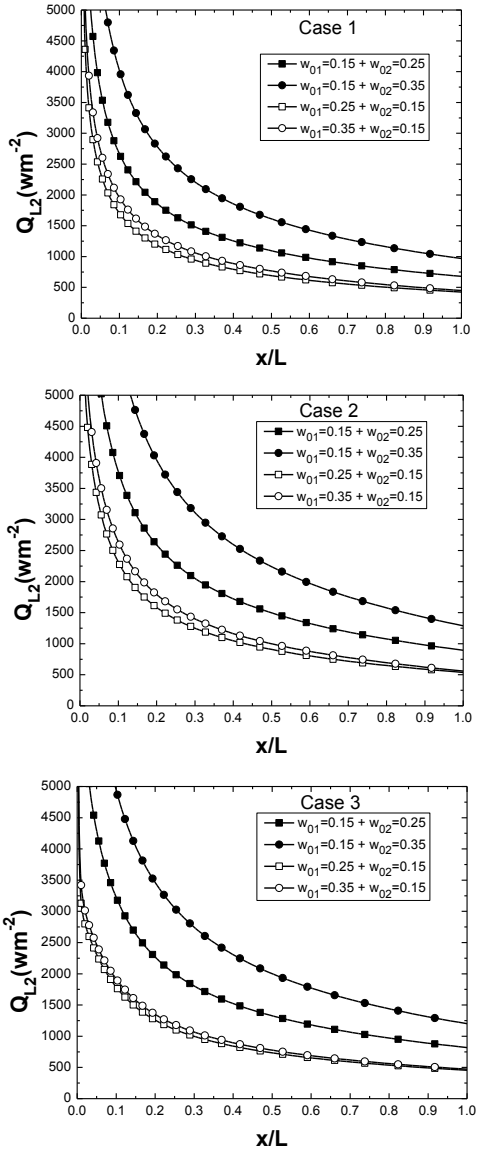

Fig. 7. Effect of inlet mass fractions w_{0i} on the latent heat flux Q_{L2} for the three cases.

4.5. Effect of the Inlet Liquid Mass flow Rate M_{0L}

To analyze the heat and mass transfer characteristics during the condensation of the studied cases, our attention is now turned to expect the effect of changing the inlet liquid mass flow rate m_{0L}. Figure 9 presents the evolution of the temperature in the two phases at different axial positions for the three cases. For this set of results, w_{01} = 0.25, w_{02} = 0.25, m_{0G} = 0.3 g.m^{-1}s^{-1}, w_{0L1} = 0.5, w_{0L2} = 0.5. It is interesting to note that for a fixed value of m_{0L}, the temperature variation in the liquid film is much lower than that in the gas, which indicates that the axial and radial terms in the liquid energy equation are not very significant. Moreover, it is noted that as the flow progresses in the tube, the temperature profiles in the liquid phase of the three cases decreases in intensity. This is due to the reduction of the heat flux by conduction, which influences the temperature at the interface (very close to the

wall temperature T_W when X = 1.0). It is also seen that in the gas region, the variation of the temperature is decreased from the axis of symmetry (η = 1.0) towards the gas-liquid interface, which proves that the heat transfer occurs from the gas to the liquid. In addition, the curve reveals that when m_{0L} is higher, the liquid film absorbs more heat, which greatly reduces the temperature of the mixture, especially for case 2 (from case 1 to case 3, the decrease of temperature is 78.17°C, 75.04°C, 82.76 °C at the tube exit, respectively). Consequently, the mass transfer to the liquid film at the interface rises, which leads to the enhancement of the condensation mechanism with a thicker liquid film thickness.

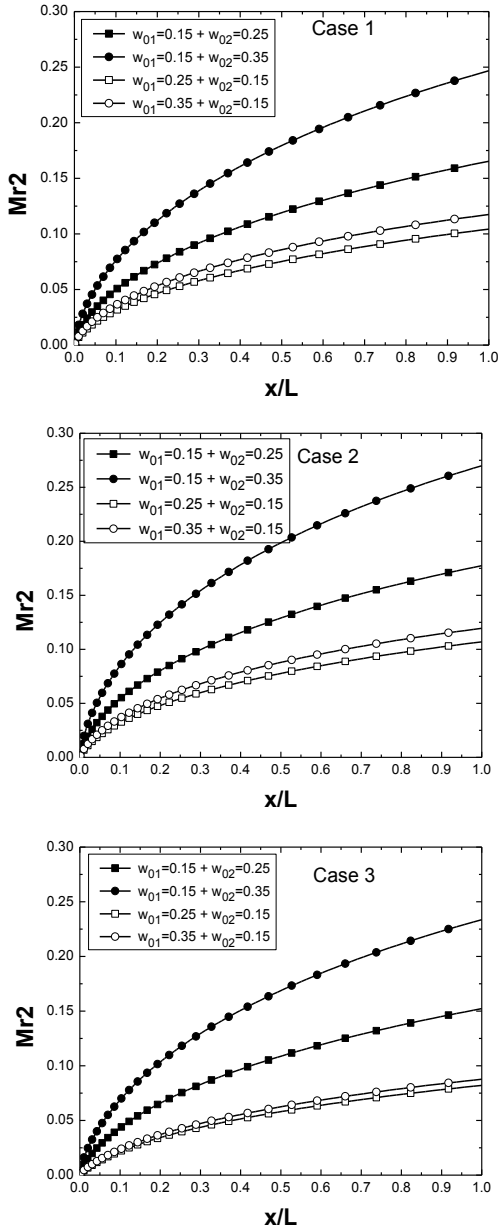

Fig. 8. Effect of inlet mass fractions w_{0i} on the accumulated condensation rate Mr2 for the three cases.

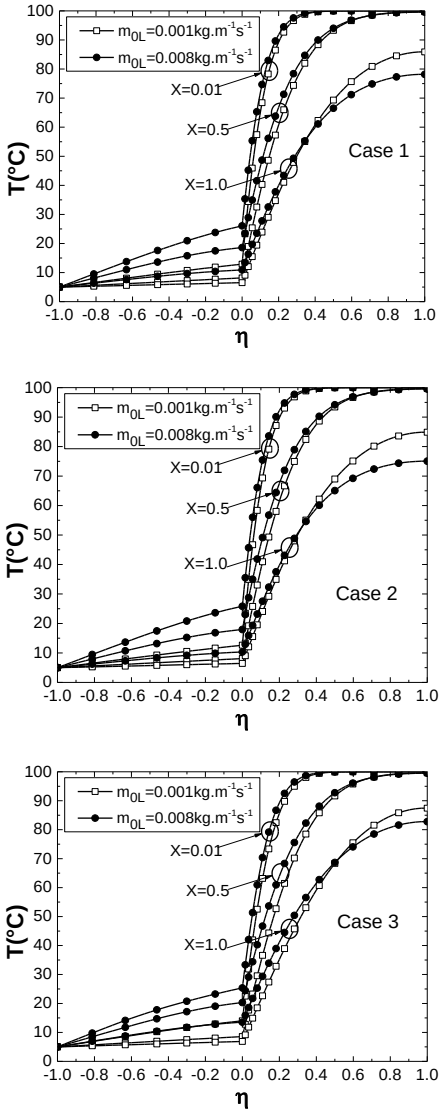

Fig. 9. Effect of inlet liquid mass flow m_{0L} on the distribution of axial temperature profile in the liquid and vapour phases at various tube sections for all cases.

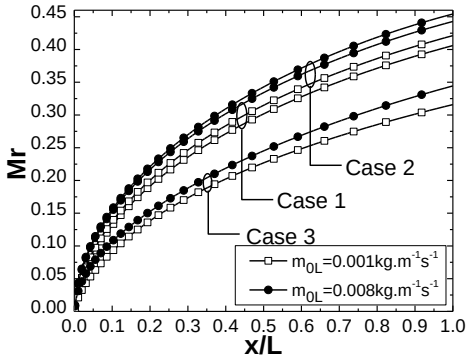

Fig. 10. Effect of inlet liquid mass flow rate m_{0L} on the variation of the total accumulated condensation rate for the three cases.

The effects of changing m_{0L} for all cases are presented in Fig. 10. This figure shows that the total accumulated condensation rate Mr increases at any

value of x/L, particularly close to the outlet of the tube. Also, a first look at the curves reveals that as the inlet liquid mass flow rate increases, Mr becomes higher all over the tube. In addition, the more the inlet liquid mass fractions increases, the more the heat transfer due to the exchange of latent heat with phase change increases. As a consequence, the concentration gradient becomes larger causing a higher condensation rate particularly for water-methanol-air mixture.

5. CONCLUSION

The numerical analysis of the present paper is conducted in order to study the combined heat and mass transfer during condensation from multicomponent mixed vapours with the presence of non-condensable gas inside a vertical tube. Results were obtained for the three cases by varying the following values of the inlet of the tube: vapour mass fractions w_{0G} and the inlet liquid mass flow rate m_{0L}. The temperature of the tube wall T_W was also analyzed. Basing on the findings of this study, the following conclusions are adopted:

- The accumulated condensation rate Mr2 of water-methanol-air is more enhanced by increasing w_{02} and for a lower wall temperature (approximately 8.5 % higher by decreasing T_W from 20 to 5°C at the tube exit).
- A higher inlet vapour mass fraction positively influences the latent heat flux Q_{L2} especially for the water-methanol-air more than water-ethanol-air ethanol-methanol-air, respectively, which improves the conjugate heat and mass exchanges.
- Water-methanol-air presents a larger accumulated condensation rate than the water-ethanol-air and ethanol-methanol-air (the growth is about 9.4 % and 15.5 % at the outlet of the tube when $w_{02} = 0.35$, respectively).
- By increasing the inlet liquid mass flow rate, the mechanism of condensation is improved along the tube, which greatly reduces the temperature of the gas mixture, especially for water-methanol-air mixture.

ANNEXE A

The thermophysical properties of the binary liquid film and ternary gas mixtures are calculated using the equations described below Poling et al. (2001).

In the liquid phase

Mixture density

$$\rho_L = \left[w_{L1}\rho_{L1} + w_{L2}\rho_{L2} \right] \quad \text{(A. 1)}$$

Mixture specific heat

$$C_{PL} = \left[w_{L1}C_{PL,1} + w_{L2}C_{PL,2} \right] \quad \text{(A. 2)}$$

Mixture dynamic viscosity

$$\mu_L = \left[Y_{L,1}\left(\mu_{L1}\right)^{\frac{1}{3}} + Y_{L,2}\left(\mu_{L2}\right)^{\frac{1}{3}} \right]^3 \quad \text{(A. 3)}$$

Mixture thermal conductivity

$$\lambda_L = \left[w_{L1}\lambda_{L1} + w_{L2}\lambda_{L2} \right] \quad \text{(A. 4)}$$

Mass diffusion of species i in species j

$$D_{L,ij} = \frac{7.4\times10^{-15}\left(\Theta_j M_j\right)^{0.5} T}{\mu_j V_i^{0.6}} \quad \text{(A. 5)}$$

Where Θ_j is the diffusion coefficient of species *i* in *j* and *Vi* is the molar weight of species *i*

Diffusion coefficient of the mixture

$$D_L\mu_L = \left[\left(D_{L,12}\mu_{L2}\right)^{Y_{L,2}} \times \left(D_{L,21}\mu_{L1}\right)^{Y_{L,1}} \right] \quad \text{(A. 6)}$$

In the gas phase

Mixture density

$$\rho_G = \frac{M_a}{RT}\left[P + P_1\left(\frac{M_1}{M_2} - 1\right) + P_2\left(\frac{M_2}{M_a} - 1\right) \right] \quad \text{(A. 7)}$$

Mixture specific heat

$$C_{pG} = \left[w_1 C_{pG,1} + w_2 C_{pG,2} + (1 - w_1 - w_2) C_{pG,a} \right] \quad \text{(A. 8)}$$

Mixture dynamic viscosity

$$\mu_G = \left[\frac{Y_1\mu_1}{Y_1 + Y_2\psi_{12} + Y_a\psi_{1a}} + \frac{Y_2\mu_2}{Y_2 + Y_1\psi_{21} + Y_a\psi_{2a}} + \frac{Y_a\mu_a}{Y_a + Y_1\psi_{a1} + Y_2\psi_{a2}} \right] \quad \text{(A. 9)}$$

Mixture thermal conductivity

$$\lambda_G = \left[\frac{Y_1\lambda_1}{Y_1 + Y_2\zeta_{12} + Y_a\zeta_{1a}} + \frac{Y_2\lambda_2}{Y_2 + Y_1\zeta_{21} + Y_a\zeta_{2a}} + \frac{Y_a\lambda_a}{Y_a + Y_1\zeta_{a1} + Y_2\zeta_{a2}} \right] \quad \text{(A. 10)}$$

Mass diffusion of species *i* in species *j*

$$D_{G,ij} = \left[\frac{0.0143T^{1.75}\left(\frac{1}{M_i} + \frac{1}{M_j}\right)^{0.5}}{PM_{ij}^{0.5}\left[\left(\sum v\right)_i^{0.33} + \left(\sum v\right)_j^{0.33}\right]^2} \right] \quad \text{(A. 11)}$$

Diffusion coefficient of species *i* in the mixture *m*

$$D_{G,1m} = \frac{1 - Y_1}{\left[\frac{Y_2}{D_{G,12}} + \frac{Y_a}{D_{G,1a}}\right]}$$

$$D_{G,2m} = \frac{1 - Y_2}{\left[\frac{Y_1}{D_{G,12}} + \frac{Y_a}{D_{G,2a}}\right]}$$

$$D_{G,\mathrm{am}} = \frac{1-Y_a}{\left[\dfrac{Y_1}{D_{G,1a}} + \dfrac{Y_2}{D_{G,2a}}\right]} \tag{A. 12}$$

Where, Y_i represents the molar fraction of the constituents i, ψ_{ij} and ζ_{ij} are the interaction parameters given as follows:

$$\psi_{ij} = \frac{\left[1+\left(\dfrac{\mu_i}{\mu_j}\right)^{\frac{1}{2}}\left(\dfrac{M_j}{M_i}\right)^{\frac{1}{4}}\right]^2}{\left[8\left(1+\dfrac{M_i}{M_j}\right)^2\right]} \tag{A. 13}$$

$$\zeta_{ij} = \frac{1.065\left[1+\left(\dfrac{\lambda_i}{\lambda_j}\right)^{\frac{1}{2}}\left(\dfrac{M_i}{M_j}\right)^{\frac{1}{4}}\right]^2}{\left[8\left(1+\dfrac{M_i}{M_j}\right)^2\right]}$$

REFERENCES

Anderson, D., J. Tannehill and R. Pletcher (1984). Computational fluid mechanics and heat transfer, Hemisphere, New York, New York.

Armou, S., R. Mir, Y. El Hammami, K. Zine-Dine and M. El Hattab (2017). Heat and Mass Transfer Enhancement in Absorption of Vapor in Laminar Liquid Film by Adding Nano-Particles. *Journal of Applied Fluid Mechanics*, 10(6), 1711-1720.

Belhadj, M. A., J. Orfi, C. Debissi, S. B. Nasrallah (2007). Condensation of water vapor in a vertical channel by mixed convection of humid air in the presence of a liquid film flowing down, *Desalination* 204, 471–481.

Charef, A., M. Feddaoui, M. Najim and H. Meftah (2017). Liquid film condensation from water vapour flowing downward along a vertical tube. *Desalination* 409, 21–31.

Dharma Rao, V., V. Murali Krishna, K. Sharma and P. M. Rao (2008). Convective condensation of vapor in the presence of a non-condensable gas of high concentration in laminar flow in a vertical pipe. *International Journal of Heat and Mass Transfer* 51, 6090–6101.

Feddaoui, M., E. Belahmidi, A. Mir and A. Bendou (2001). Numerical study of the evaporative cooling of liquid film in laminar mixed convection tube flows. *International Journal of Thermal Sciences* 40(11), 1011–1020.

Hassaninejadfarahani, F., M. Guyot and S. Ormiston (2014). Numerical analysis of mixed-convection laminar film condensation from high air mass fraction steam-air mixtures in vertical tubes. *International Journal of Heat and Mass Transfer* 78, 170–180.

Jiang, R., X. Ma, Z. Lan, Y. Bai and T. Bai (2015). Visualization study of condensation of ethanol water mixtures in trapezoidal microchannels. *International Journal of Heat and Mass Transfer* 90, 339–349.

Krishna, R. and C. Panchal (1977). Condensation of a binary vapour mixture in the presence of an inert gas. *Chemical Engineering Science* 32, 7, 741–745.

Krishna, R. (1979). Effect of nature and composition of inert gas on binary vapour condensation. *Letters in heat and Mass Transfer* 6, 2, 137–147.

Kubin, M., J. Hirs and J. Plasek (2016). Experimental analysis of steam condensation in vertical tube with small diameter. *I. J. Heat Mass Transfer* 94, 403–410.

Lebedev, P., A. Baklastov and Z. Sergazin (1969). Aerodynamics, heat and mass transfer in vapour condensation from humid air on a flat plate in a longitudinal flow in asymmetrically cooled slot. *International Journal of Heat and Mass Transfer* 12(8), 833–841.

Li, Y., J. Yan, L. Qiao and S. Hu (2008). Experimental study on the condensation of ethanol water mixtures on vertical tube. *Heat and Mass Transfer* 44, 5, 607–616.

Ma, X., Z. Lan, W. Xu, M. Wang and S. Wang (2012). Effect of surface free energy difference on steam-ethanol mixture condensation heat transfer. *International Journal of Heat and Mass Transfer* 55(4), 531–537.

Najim, M., M. Feddaoui, A. Charef and H. Meftah, (2017). Computational study of saline water film evaporation in a vertical tube. *Desalination* 408, 81–91.

Nasr, A. and A.S. El-ghamdi (2017). Evaporation and condensation of falling binary liquid film. *Thermal science* 21, 1A, 211-222.

Nasr, A. and A.S. El-ghamdi (2017) Simultaneous heat and mass transfer during evaporation and condensation of a binary liquid film. Thermal science.

Nasr, A., C. Debbissi and S. B. Nasrallah (2011). Evaporation of a binary liquid film by forced convection. *Thermal science* 15, 773-784.

Patankar, S., *Numerical heat transfer and fluid flow*, hemisphere/mcgraw-hill, New York, 1980.

Perry, R., Green, D., *Perry's chemical engineers handbook*, McGraw-Hill. New York, 1997.

Poling, B. E., J. M. Prausnitz, O. John Paul and R. C. Reid (2001). *The* properties *of gases and liquids*, Vol. 5, New York.

Raithby, G. D. and G. E. Schneider (1979), Numerical solution of problems in incompressible fluid flow: treatment of the velocitypressure coupling, *Numerical Heat*

Transfer 2 4, pp. 417–440.

Ralston, A. and P. A. Rabinowitz (2001*) first course in numerical analysis*, Courier Corporation.

Siow, E., S. Ormiston and H. Soliman (2004). A two-phase model for laminar film condensation from steam-air mixtures in vertical parallel-plate channels. *Heat and Mass Transfer* 40(5), 365–375.

Taitel, Y. and A. Tamir (1974). Film condensation of multicomponent mixtures, *International Journal of Multiphase Flow* 1(5), 697–714.

Utaka, Y. and S. Wang (2004). Characteristic curves and the promotion effect of ethanol addition on steam condensation heat transfer. *International Journal of Heat and Mass Transfer* 47(21), 4507–4516.

Wang, J., J. Yan, S. Hu and J. Liu (2009). Marangoni condensation heat transfer of water ethanol mixtures on a vertical surface with temperature gradients. *International Journal of Heat and Mass Transfer* 52, 2324–2334.